Final Technical Report

Fundamental Physics and Practical Applications of Electromagnetic Local Flow Control in High Speed Flows

AFOSR Grant FA9550-07-1-0228

Period of Grant: 1 April 2007 - 30 November 2009

Prof. Doyle D. Knight and Mrs. Kellie Anderson
Department of Mechanical and Aerospace Engineering
Rutgers - The State University of New Jersey
98 Brett Road
Piscataway, New Jersey 08854
Phone: 732 445 4464 · Fax: 732 445 3124
Email: doyleknight@gmail.com

Submitted to:
Dr. John Schmisseur
Air Force Office of Scientific Research
875 North Randolph Street, Room 3112
Arlington, Virginia 22203
Phone: 703 696 6962 · Fax: 703 696 8451
Email: John.Schmisseur@afosr.af.mil

22 February 2010

Report Documentation Page

Form Approved
OMB No. 0704-0188

1. REPORT DATE	2. REPORT TYPE	3. DATES COVERED
22 FEB 2010		**01-04-2007 to 30-11-2009**

4. TITLE AND SUBTITLE	5a. CONTRACT NUMBER
Fundamental Physics and Practical Applications of Electromagnetic Local Flow Control in High Speed Flows	5b. GRANT NUMBER
	5c. PROGRAM ELEMENT NUMBER
6. AUTHOR(S)	5d. PROJECT NUMBER
	5e. TASK NUMBER
	5f. WORK UNIT NUMBER
7. PERFORMING ORGANIZATION NAME(S) AND ADDRESS(ES) **Department of Mechanical and Aerospace Engineering,Rutgers - The State University of New Jersey,98 Brett Road,Piscataway,NJ,08854**	8. PERFORMING ORGANIZATION REPORT NUMBER
9. SPONSORING/MONITORING AGENCY NAME(S) AND ADDRESS(ES)	10. SPONSOR/MONITOR'S ACRONYM(S)
	11. SPONSOR/MONITOR'S REPORT NUMBER(S)

12. DISTRIBUTION/AVAILABILITY STATEMENT
Approved for public release; distribution unlimited

13. SUPPLEMENTARY NOTES

14. ABSTRACT

15. SUBJECT TERMS

16. SECURITY CLASSIFICATION OF:			17. LIMITATION OF ABSTRACT	18. NUMBER OF PAGES	19a. NAME OF RESPONSIBLE PERSON
a. REPORT	b. ABSTRACT	c. THIS PAGE			
unclassified	**unclassified**	**unclassified**	**Same as Report (SAR)**	**19**	

REPORT DOCUMENTATION PAGE

Form Approved
OMB No. 0704-0188

PLEASE DO NOT RETURN YOUR FORM TO THE ABOVE ADDRESS.

1. REPORT DATE *(DD-MM-YYYY)*	2. REPORT TYPE	3. DATES COVERED *(From - To)*
22-02-2010	Final Technical	1 April 2007 - 30 November 2009

4. TITLE AND SUBTITLE

Fundamental Physics and Practical Applications of Electromagnetic Local Flow Control in High Speed Flows

5a. CONTRACT NUMBER

5b. GRANT NUMBER

FA9550-07-1-0228

5c. PROGRAM ELEMENT NUMBER

6. AUTHOR(S)

Doyle D. Knight and Kellie Anderson

5d. PROJECT NUMBER

5e. TASK NUMBER

5f. WORK UNIT NUMBER

7. PERFORMING ORGANIZATION NAME(S) AND ADDRESS(ES)

Department of Mechanical and Aerospace Engineering
Rutgers - The State University of New Jersey
98 Brett Road
Piscataway, New Jersey 08854

8. PERFORMING ORGANIZATION REPORT NUMBER

CCD 2010-1

9. SPONSORING/MONITORING AGENCY NAME(S) AND ADDRESS(ES)

Air Force Office of Scientific Research
875 North Randolph Street, Room 3112
Arlington, Virginia 22203

10. SPONSOR/MONITOR'S ACRONYM(S)

11. SPONSOR/MONITOR'S REPORT NUMBER(S)

12. DISTRIBUTION/AVAILABILITY STATEMENT

Unclassified; Distribution Unlimited

13. SUPPLEMENTARY NOTES

14. ABSTRACT

The report summarizes two major achievements in Electromagnetic Local Flow Control (ELFC) in high speed flows. The first achievement is the demonstration of the effective and efficient reduction of pressure drag on a blunt cylinder in supersonic flow using pulsed heated filaments. Numerical simulations indicate drag reduction up to 30% with power requirements typically 1% of the power saved through drag reduction. No adverse effect on heat transfer to the blunt cylinder is observed. Indeed, a 30% reduction in heat transfer is observed for one configuration. The second achievement is the development and application of a fully 3-D, time-accurate, viscous gas dynamic code for simulation of microwave energy discharge in air (including full thermochemistry) and the interaction of the microwave-generated plasma with a blunt body in supersonic flow. Comparison of computed and experimental surface pressure show good agreement.

15. SUBJECT TERMS

Hypersonic, supersonic, plasma, computational fluid dynamics

16. SECURITY CLASSIFICATION OF:			17. LIMITATION OF ABSTRACT	18. NUMBER OF PAGES	19a. NAME OF RESPONSIBLE PERSON
a. REPORT	b. ABSTRACT	c. THIS PAGE			Doyle Knight
U	U	U	UU	17	19b. TELEPHONE NUMBER *(Include area code)* 732 445 4464

Abstract

The report summarizes a research program focused on the understanding of the fundamental physics and practical applications of Electromagnetic Local Flow Control (ELFC) in high speed flows. ELFC encompasses a wide variety of energy deposition techniques (*e.g.*, plasma arcs, laser pulse, microwave, electron beam, glow discharge, etc) both with and without magnetic field, and a wide range of applications (*e.g.*, drag reduction, lift and moment enhancement, improved combustion and mixing, modification of shock structure, etc.). This report summarizes two main research achievements in the area of ELFC. The first is a study of the efficiency and effectiveness of energy deposition in reducing drag on a blunt body, and the concommitant effect on heat transfer to the body. A computational study of the interaction of energy deposition on a blunt cylinder was performed for varying filament pulse periods. The results indicate that energy deposition is both effective in reducing drag on blunt bodies in supersonic flow, and also efficient in the sense that the power required is significantly less than the power saved. Moreover, no adverse effects on heat transfer to a blunt body were observed, and in one case a significant reduction in heat transfer was achieved. The second is the development of a fully three-dimensional, time-dependent gas dynamic code for microwave energy deposition in air incorporating detailed kinetics and thermochemistry. This code is validated by means of a comparison to experimental data, and is used to analyze interaction of a plasma filament with a hemisphere cylinder and a hemisphere-cone cylinder. To the authors' knowledge, this is the only code with the capability for simulating both the full thermochemistry of microwave discharge in air and the interaction of the microwave-generated plasma with an aerodynamic shape.

I. Introduction

In recent years there has been intense research activity in developing fundamental understanding and practical applications of Electromagnetic Local Flow Control (ELFC). The term Electromagnetic Local Flow Control encompasses a wide range of energy deposition techniques including beamed energy deposition (*i.e.*, electron beam, laser, and microwave, in the sense that each represents beamed electromagnetic radiation) and DC discharge (in the sense of energy deposition by means of an imposed electric field), either with or without external magnetic fields. This interest is reflected in numerous conferences and workshops including the Weakly Ionized Gas Workshops (since 1997), the St. Petersburg Workshops (since 2000) and the IVTAN Workshops (since 1999). ELFC research encompasses a wide variety of energy deposition techniques (*e.g.*, plasma arcs, laser pulse, microwave, electron beam, glow discharge, etc) both with and without magnetic field, and a wide range of applications (*e.g.*, drag reduction, lift and moment enhancement, improved combustion and mixing, modification of shock structure, etc.). Reviews of this research include Shang,[1] Knight *et al*,[2] Fomin *et al*,[3] Knight,[4] Bletzinger *et al*[5] and Knight.[6]

The advantages of Electromagnetic Local Flow Control are twofold. First, the actuation times are comparable or substantially smaller than the flowfield development times in supersonic and hypersonic flight. For example, consider a hypersonic vehicle operating at Mach 6 and 30 km altitude. The relevant timescale for flowfield development in the vicinity of an $l = 10$ cm dimension (*e.g.*, a cowl leading edge radius) is $l/U_\infty = 5.5 \cdot 10^{-5}$ s. Typical pulse durations for laser and microwave are $\mathcal{O}(10^{-8}$ s) and $\mathcal{O}(10^{-5}$ s), respectively, thereby permitting modification of the local flowfield. Electromechanical or mechanical flow control systems, however, are much slower with characteristics actuation times that are $\mathcal{O}(10^{-2}$ s). Second, beamed energy deposition can be effectively used to modify the flowfield at large distances from the energy source (*i.e.*, at distances from the vehicle), whereas electromechanical or mechanical flow control systems are limited to modifying the flow in the immediate vicinity of the vehicle.

Plasmadynamics is an inherent element in Electromagnetic Local Flow Control. Typical methods of energy deposition in air by electromagnetic techniques (*e.g.*, DC discharge, electron beam, laser and microwave) generate a high temperature plasma with ions (N_2^+, O_2^+, NO^+, N^+, etc), electrons (e), dissociated species (N, O), excited states ($N_2(A^3\Sigma_u+)$, $N_2(B^3\Pi_g)$, etc) and molecules (NO) in addition to N_2 and O_2. The formation of the plasma (*e.g.*, its shape and structure) has an important effect on its ability to modify the flowfield.

For example, microwave energy deposition in air generates a plasma characterized by a "warm" region whose size is on the order of the microwave wavelength and which contains thin "hot" filaments whose diameter is one to two orders of magnitude smaller (Fig. 1). Detailed experiments and computations have demonstrated that the interaction of the microwave-generated plasma with a blunt body in supersonic flow can lead to a momentary reduction in drag principally due to the interaction of the filaments with the blunt body shock (Kolesnichenko *et al*,[7–10] and Wilkerson *et al*[11]).

Figure 1. Microwave filaments

This report summarizes two main research achievements in the area of ELFC. The first is a study of the efficiency and effectiveness of energy deposition in reducing drag on a blunt body, and the concommitant effect on heat transfer to the body. A computational study of the interaction of energy deposition and a blunt cylinder is performed for varying filament pulse periods. This study is detailed in Section II. The second is the development of a fully three-dimensional, time-dependent gas dynamic code for microwave energy deposition in air incorporating detailed kinetics and thermochemistry. This code is validated by means of a comparison to experimental data, and is used to analyze interaction of a plasma filament with a hemisphere cylinder and a hemisphere-cone cylinder. These results are presented in Section III.

II. Effectiveness, Efficiency and Heat Transfer Effects of Energy Deposition for Flow Control

A computational study was performed to examine the interaction of a periodic sequence of heated filaments with a blunt cylinder in supersonic flow. The heated filaments are introduced on the axis of symmetry upstream of the cylinder and aligned with the freestream flow. The heated filaments are an idealization of the filamentary plasma structures generated by a microwave discharge in air (Fig. 1). The interaction is examined with a focus on two effects, namely, 1) the efficiency and effectiveness of drag reduction, and 2) the effect on heat transfer to the cylinder face. The configuration is shown in Fig. 2. The value of the freestream Reynolds number $Re = \rho_\infty U_\infty D/\mu_\infty$ is chosen to approximate typical experimental values, such as experiments performed by Kolesnichenko *et al*[12] where typical values for p_∞, T_∞ and D are 25-50 Torr, 155 K, and 20-40 mm, respectively. The flow parameters are defined in Table 1. Note that the fixed cylinder surface temperature T_w exceeds the adiabatic wall temperature T_a by 11% (hot wall). The pulse period L/D is varied from 4/3 to infinitely long.

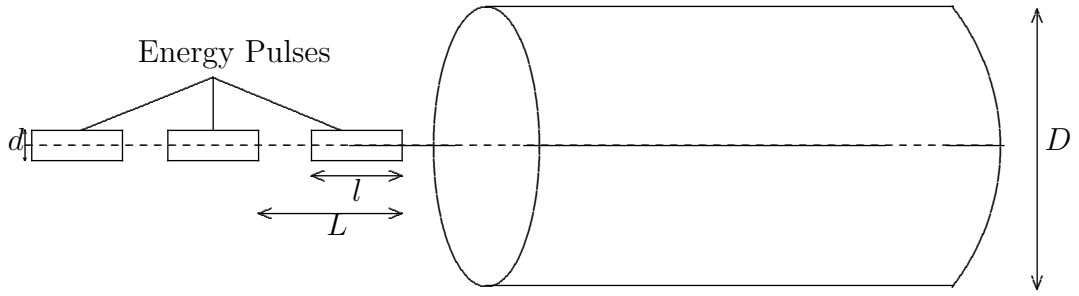

Figure 2. Computational domain

The heated filaments are defined by the density ratio $\alpha = \rho_f/\rho_\infty$ (where ρ_f is the filament density), diameter ratio d/D, length ratio l/D and period L/D. Fixed values of $\alpha = 0.5$ and $l/D = 1$ (except for the infinitely long filament) were assumed. The filaments are introduced at the inflow boundary of the computational domain with static pressure $p_f = p_\infty$ and velocity $U_f = U_\infty$. The temperature of the filament is therefore $T_f = \alpha^{-1} T_\infty$.

The governing equations are the unsteady laminar compressible Navier Stokes equations for an ideal gas. The flow is axisymmetric. The molecular viscosity is defined by Sutherland's Law. A code was written in C++ to solve the governing equations using a finite volume

Table 1. Flow Parameters

Type	Description	Definition	Value
Dimensionless Flow	Mach	M_∞	1.89
	Specific heat ratio	γ	1.4
	Reynolds number	Re	$7.0 \cdot 10^4$
	Prandtl number	Pr	0.7
Dimensionless Filament	Density ratio	α	0.5 all cases
	Diameter	$\frac{d}{D}$	0.1 all cases
	Length	$\frac{l}{D}$	1.0, 1.0, 1.0, ∞
	Pulse (Period)	$\frac{L}{D}$	$\frac{4}{3}$, 2.0, 4.0, ∞
Cylinder	Temperature	T_w/T_∞	2.0 all cases
	Adiabatic Wall Temperature	T_a/T_∞	1.8

method. Details of the code are given in Anderson.[13] Van Leer's flux splitting method[14] is used for the inviscid fluxes. The viscous fluxes are solved with a second order accurate discretization. The conservative variables are reconstructed using a third order accurate Essentially Non-Oscillatory (ENO) Method.[15] A second order accurate explicit Runge-Kutta scheme is used to integrate in time.[16] The code is parallelized using Message Passing Interface (MPI). The corner of the cylinder creates a local singularity to the flow. To minimize errors introduced by the singularity, an entropy fix proposed by Woodward *et al*[17] was incorporated to the code. For the larger period cases ($L/D = 2$ and $L/D = 4$), the density and pressure were relaxed in time if the computed density in the vicinity of the corner was momentarily negative. The density and pressure were set equal to a weighting between the computed parameters from the current timestep to the computed parameters from the previous step in the Runge-Kutta scheme.

The computational domain is shown in Fig. 3. The pulses have the greatest effect at the face of the cylinder. Therefore, only one cylinder diameter in length of the body was included in the flow domain. The height of the domain extends two and a half cylinder diameters above the body. The blunt body shock is expected to lense forward upon interaction with the heated filaments based on trial runs, and consequently the upstream boundary of the flow domain is two cylinder diameters in length in front of the body.

The principal measures of aerodynamic performance associated with the interaction of the heated filaments with the blunt cylinder are the *efficiency* and *effectiveness* of the drag reduction. The efficiency is defined as the ratio of the power saved due to drag reduction by the heated filament to the power necessary to create the heated filament. The efficiency is obtained by dividing the average thrust power saved due to the filament divided by the power used to create the filament. The efficiency of drag reduction in terms of dimensionless variables is

$$\eta = \frac{8(\gamma-1)M_\infty^2}{1-\alpha}\left(\frac{D}{d}\right)^2 \frac{D}{l}\int_0^{L/D}\int_0^{1/2}(p_o - p)r\,dr\,dt \tag{1}$$

where the pressure is nondimensionalized by $\rho_\infty U_\infty^2$, the subscript o indicates the absence of the filament and $l/D = L/D = \tau_\infty$ for $L/D = \infty$. Derivation of this expression may be found in Anderson.[13]

The effectiveness is defined as the ratio of the average frontal drag reduction due to the

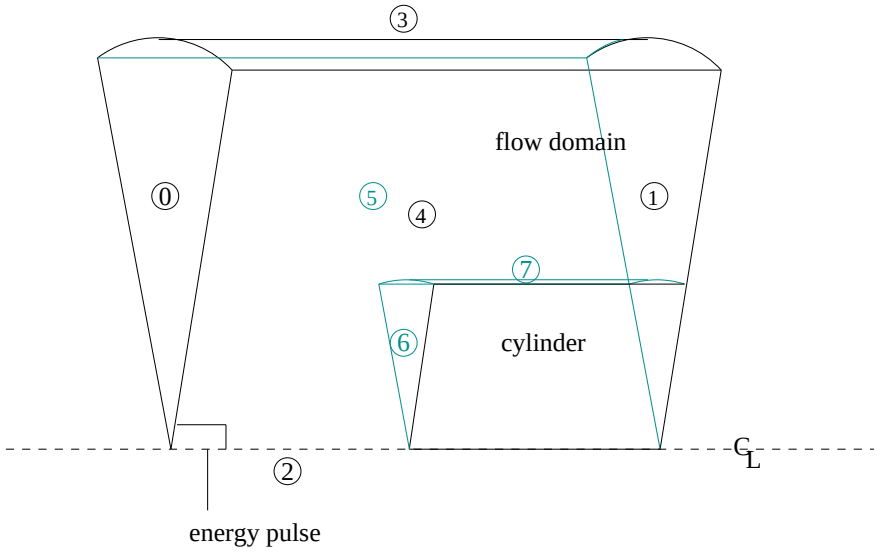

Figure 3. Axisymmetric wedge solution domain

presence of the filament to the frontal drag in the absence of the filament. The effectiveness is

$$\zeta = \frac{\int_0^{L/D} \int_0^{1/2} (p_o - p) r dr dt}{L/D \int_0^{1/2} p_o r dr} \tag{2}$$

where $L/D = \tau_\infty$ for $L/D = \infty$.

The principal measure of aerothermodynamic performance associated with the interaction of the heated filaments with the blunt cylinder is the ratio Φ of the average heat transfer on the cylinder face due to the interaction with the filaments to the heat transfer on the cylinder face in the absence of the filaments.

$$\Phi = \frac{\overline{Q}_{fil}}{\overline{Q}_{nofil}} \tag{3}$$

where

$$\overline{Q} = \frac{1}{\tau} \int_0^\tau \int_0^{1/2} q_w r dr dt \tag{4}$$

where τ is the time interval non-dimensionalized by D/U_∞ at which the integral is taken, r is the radius, non-dimensionalized by the cylinder diameter, and q_w is the heat flux to the cylinder face non-dimensionalized by $\rho_\infty U_\infty^3$. A positive heat flux implies cooling of the cylinder face. The sensitivity of the heat transfer ratio to the grid size was determined. For each pulse period evaluated, two grids were allowed to reach a statistically stationary state, the second with cell sizes half the size of the initial. The error of the refined grid is calculated based on these two cases to determine the accuracy of the computations. The estimated uncertainty in Φ in the refined grid is less than 6%.

The efficiency η, effectiveness ζ and heat transfer parameter Φ *vs* pulse period L/D are presented in Figs. 4, 5, and 6, respectively. The overall efficiency is very high with typical values approximately 100 (*i.e.*, for every Watt of power supplied to heat the filament, more than 100 Watts of thrust power are saved) with a maximum value at $L/D = 2$. The extraordinarily large values of efficiency are consistent with the analysis of Kolesnichenko *et al.*[18] Substantial levels of drag reduction up to 30% are achieved with pulsed filaments. The

effectiveness decreases with increasing period as expected since fewer filaments interact with the blunt cylinder per unit time.

A major concern is the effect of the heated filaments on the heat transfer to the cylinder face. It is notable that the heat transfer parameter Φ does not exceed unity implying that there is no increase in average heat transfer to the blunt cylinder face. Indeed, the heat transfer is *reduced* for the $L/D = 4/3$ case. The reason for the minimum heat transfer at $L/D = 4/3$ is discussed below in terms of the vortex structure.

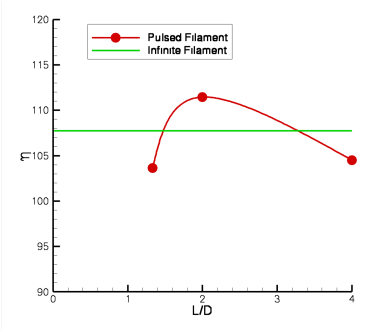

Figure 4. Efficiency

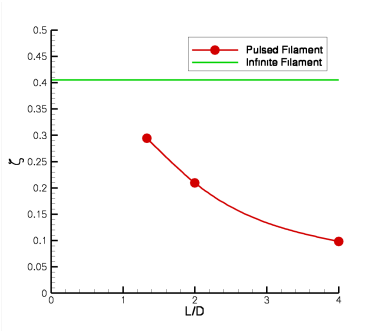

Figure 5. Effectiveness

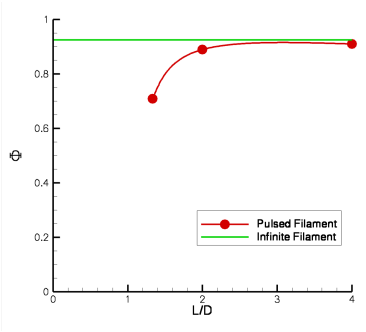

Figure 6. Heat Transfer

Contours of velocity magnitude and instantaneous streamlines are shown in Fig. 7 for $L/D = \infty$. The interaction of the filament with the blunt body shock generates an unstable shear layer (identified by the abrupt change in color from blue [low speed] to green [high speed] in Fig. 7) resulting in the formation of sequence of periodic vortices. As the line of vortices interacts with the cylinder face, two quasi-stationary vortical structures are established. A counter-clockwise rotating vortex forms just below the line of vortices (CCW vortex) and a clockwise rotating vortex (CW vortex) develops beneath it (see Farzan *et al.*[19] The size and location of the vortices vary in time, but their presence ahead of the cylinder face is maintained. Instantaneous streamlines from the freestream above the high temperature filament remain above the line of vortices. This deflection of streamlines creates a perceived streamlining of the body and is responsible for the reduction in drag.

The pulsed filament case with a period of $L/D = 4/3$ demonstrates the greatest reduction in average heat transfer to the cylinder face (Fig. 6). The contours of the velocity magnitude and the instantaneous streamlines are shown in Fig. 8. Each pulsed filament generates a vortex behind the bow shock. The proximity of the vortices is sufficient to provide streamlining for the majority of the heat transfer cycle, which creates a stagnation region below the line of vortices. The nearly stagnant flow warms to the cylinder temperature, creating a thermal layer at the cylinder face. This quasi-stationary thermal layer then decreases heat transfer from the cylinder surface. The vortices established in the infinitely long filament case are not generated in this case. This is likely due to a brief break between streamlining of the vortices, which sweeps flow ahead of the cylinder over the corner. Thus, the heat transfer is reduced further for this case than the infinitely long filament case.

The velocity magnitude contours and instantaneous streamlines for the periodic energy deposition case with a period of $L/D = 2$ are shown in Fig. 9. The integrated heat transfer is close to unity for this case. The vortices provide a partial streamlining, which allows for a heated layer to build ahead of the cylinder face. The time between filaments, however, is sufficiently large that the heated layer is convected away from the body, thereby introducing cooler flow into the region ahead of the cylinder face and increasing the heat transfer. The time between streamlining is much greater than the time the streamlining creates a thermal

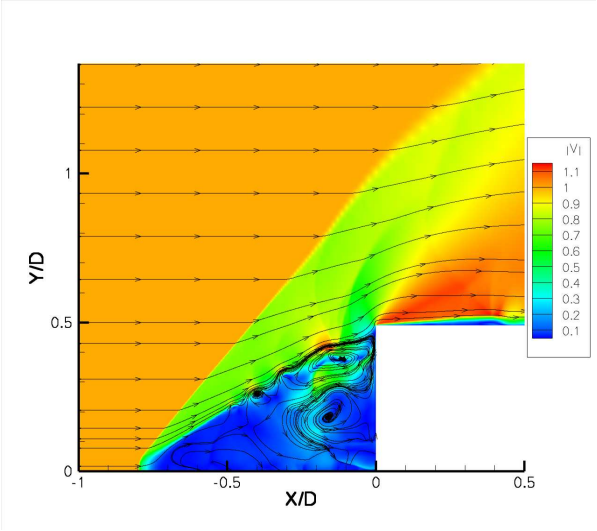

Figure 7. $L/D = \infty$

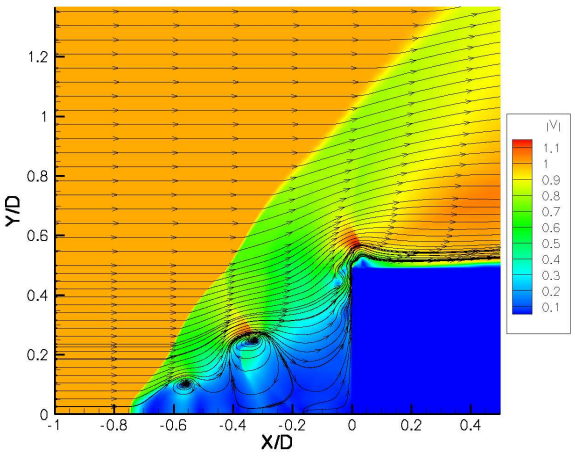

Figure 8. $L/D = 4/3$

layer, thus the integrated heat transfer is not greatly reduced.

The case of the pulsed filament with $L/D = 4$ exhibits a heat transfer parameter $\Phi \approx 1$. The velocity magnitude contours and instantaneous streamlines are shown in Fig. 10. Although the vortices temporarily streamline the body and allow for partial warming of the flow ahead of the cylinder face, the time between vortices is large compared to the time wherein the vortex streamlines the flow. Hence, the heat transfer is close to one, similar to the pulsed period of two case.

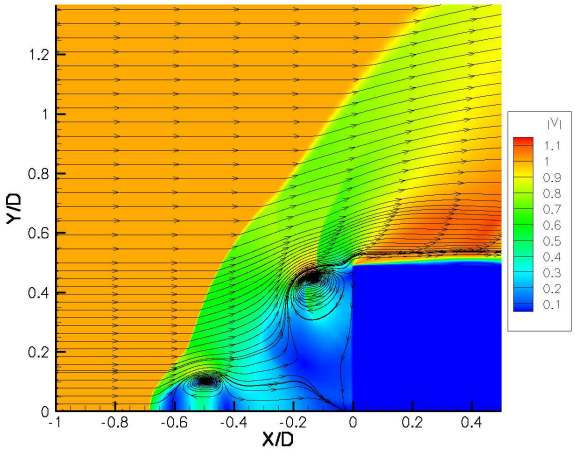

Figure 9. $L/D = 2$

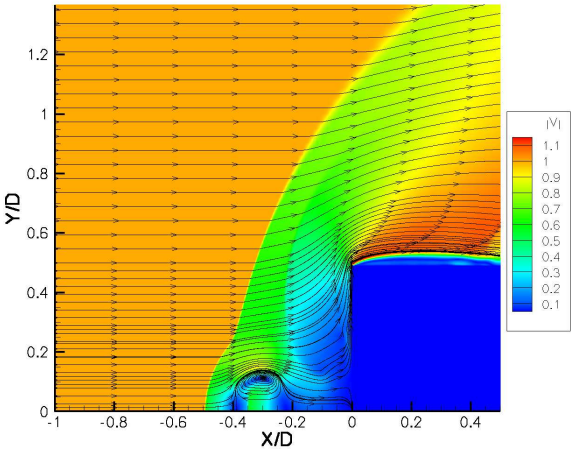

Figure 10. $L/D = 4$

III. Interaction of Microwave-generated Plasma with Blunt Aerodynamic Shapes

A fully three-dimensional, time-dependent, viscous gas dynamic code for simulating microwave energy deposition in air has been developed incorporating detailed kinetics and thermochemistry. The governing equations and thermochemistry model are described in Knight*et al.*[20] The code is written in C++ and parallelized using Message Passing Interface (MPI). *To the authors' knowledge, this is the only code with the capability for simulating both the full thermochemistry of microwave discharge in air and the interaction of the microwave-generated plasma with an aerodynamic shape.* The thermochemistry model was developed in the laboratory of Dr. Yuri Kolesnichenko (Joint Institutes for High Temperatures, Moscow, Russia). The code was validated by comparison to experimental data for the interaction of a microwave-generated plasma with a hemisphere-cylinder and hemisphere-cone-cylinder.

A. Plasma Interaction with Hemisphere Cylinder

The gas dynamic code is applied to the simulation of the interaction of a microwave-generated plasma with the flow past a hemisphere-cylinder at $M_\infty = 2.1$. Fig. 11 displays the flow configuration which is axisymmetric. The microwave pulse is focused at a distance x_o upstream of the center of curvature of the hemisphere. The freestream conditions are listed in Table 2. The inflow corresponds to standard air at the specified static pressure and temperature with the inclusion of a small concentration of electrons N_e and molecular oxygen ions $N_{O_2^+}$. The freestream concentration of all other species is set to zero. The microwave parameters are indicated in Table 3.

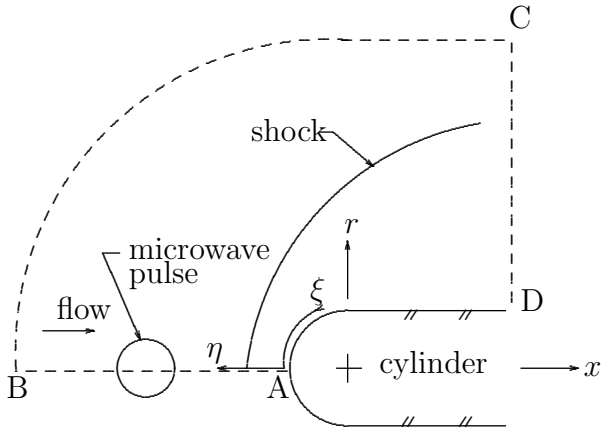

Figure 11. Computational domain

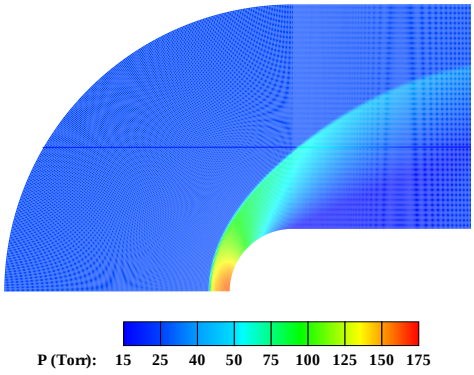

Figure 12. Initial condition for MW pulse

Details of the grids are listed in Table 4 and discussed in Knight *et al.*[21] The number of cells N_ξ and N_η in the ξ- and η-directions, respectively, are indicated, together with the total number of cells N_{total} in the computational domain. The number of processors $N_p = 36$. Axis boundary conditions are applied on the symmetry axis AB. Freestream conditions are imposed on the outer boundary BC, and zero gradient conditions at the outflow boundary CD. Tangential (slip) boundary conditions are applied on the hemisphere-cylinder surface AD since the flow was assumed inviscid for this configuration. The initial condition for the microwave pulse is the converged solution for flow past the body at the freestream conditions shown in Table 2. The initial computed static pressure contours are shown in Figs. 12.

Table 2. Freestream Conditions

Quantity	*Value*
M_∞	2.1
p_∞ (Torr)	26
T_∞ (K)	154
D (cm)	2.0
N_{N_2} (cm^{-3})	$1.287 \cdot 10^{18}$
N_{O_2} (cm^{-3})	$3.422 \cdot 10^{17}$
$N_{O_2^+}$ (cm^{-3})	$3.0 \cdot 10^4$
N_e (cm^{-3})	$3.0 \cdot 10^4$

Table 3. Microwave Parameters

Quantity	*Value*
E_o (kV/cm)	2.3
λ (cm)	3.33
f (GHz)	9.0
τ_o (μs)	1.20
τ_1 (μs)	1.21
x_o (cm)	-3.5

Table 4. Details of Grids

Quantity	*Grid No. 1*	*Grid No. 2*
N_ξ	276	550
N_η	90	180
N_{total}	24,840	99,000
$\Delta r_{\min}$ (cm)	$4.00 \cdot 10^{-2}$	$2.00 \cdot 10^{-2}$
$\Delta r_{\max}$ (cm)	$4.00 \cdot 10^{-2}$	$2.00 \cdot 10^{-2}$
$\Delta s_{\min}$ (cm)	$1.13 \cdot 10^{-2}$	$0.57 \cdot 10^{-2}$
$\Delta s_{\max}$ (cm)	$5.86 \cdot 10^{-2}$	$2.95 \cdot 10^{-2}$
N_p	36	36

The development of the pressure p, temperature T and electron temperature T_e at the center of the discharge is shown in Fig. 13. Also shown is the imposed electric field $E_o f(t)$ and reduced field $E/\mathcal{N}$ at the center. The pressure reaches a maximum value of 346 Torr at $t = 1.4$ μs, and the gas temperature reaches a maximum of 1958 K at $t = 1.4$ μs. The maximum reduced field is 135 Td. The contributions to the gas heating q_{elastic}, q_{joule}, and $q_{\text{reactions}}$ at the center of the discharge are shown in Fig. 14. The most significant contribution is $q_{\text{reactions}}$ which reaches a maximum value of 1.25 MW/cm^3 at $t = 1.2$ μs. The corresponding maximum values for q_{joule} and q_{elastic} are 0.19 MW/cm^3 and 0.019 MW/cm^3. Note that the rotational relaxation factor ν is on the order of 10^{-2} for a reduced field of 100 Td, thereby accounting for the low level of Joule heating. The Joule heating term becomes zero at the termination of the pulse since the electric field vanishes. Since the collision frequency ν_e is an assumed function of the reduced field, the elastic heating also goes to zero when the electric field vanishes. Overall, the principal contribution to the gas heating is due to the thermochemical reactions (*i.e.*, the quenching of excited states).

Details of the kinetics of the plasma formation are illustrated in Figs. 15 and 16 which display the evolution of the concentration (cm^{-3}) of selected species at the center of the plasma for $t = 0$ to $t = 2$ μs. Fig. 15 indicates a modest dissociation of N_2 with a peak value of N equal to 3.6% of the freestream N_2 concentration. The concentration of the

electronically excited states of nitrogen $N(^2D)$, $N(^2P)$, $N_2(a'^1\Sigma_u^-)$, $N_2(A^3\Sigma_u+)$, $N_2(B^3\Pi_g)$, $N_2(C^3\Pi_u)$ do not exceed $4 \cdot 10^{16}$ cm^{-3} (*i.e.*, 3.1% of the freestream N_2 concentration) and rapidly decay (Figs. 15 and 16).

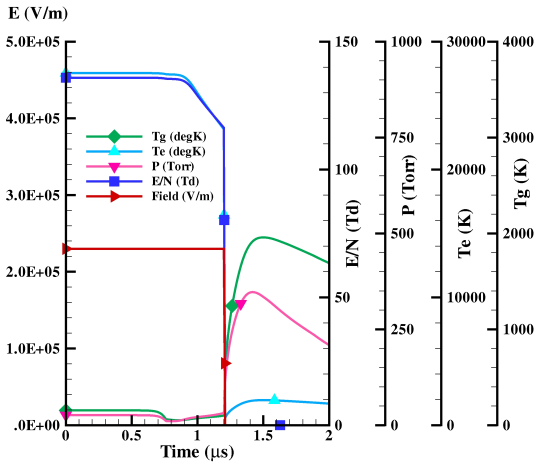

Figure 13. p, T, T_e *vs* t

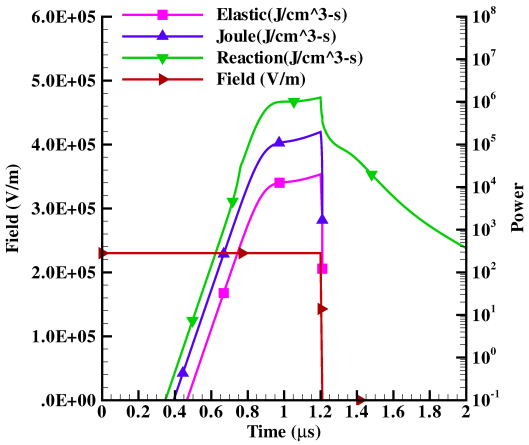

Figure 14. Heating terms

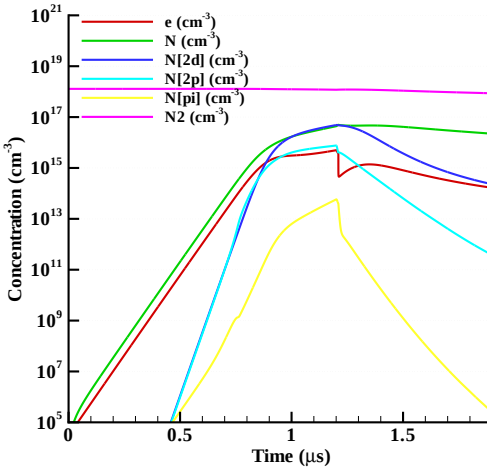

Figure 15. Plasma species

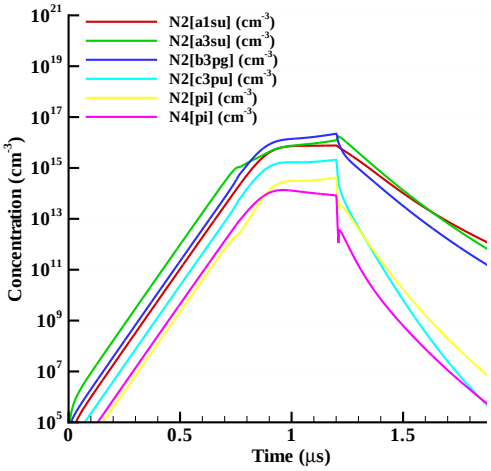

Figure 16. Plasma species

The computed and experimental surface pressure *vs* time on the centerline of the body surface for the hemisphere-cylinder are shown in Fig. 17. The natural frequency of the experimental pressure transducer is approximately 120 kHz and therefore the computed surface pressure was filtered to simulate the experimental measurement. The filtering was performed by multiplying the Fourier coefficients of the computed surface pressure time series by a factor $c(f)$ where

$$c(f) = \begin{cases} 1 & 0 \le f \le f_1 \\ 1 - (f - f_1)/(f_2 - f_1) & f_1 \le f \le f_2 \\ 0 & f_2 < f \end{cases} \tag{5}$$

where $f_1 = 30$ kHz and $f_2 = 60$ kHz. The time point of initial pressure decrease was matched between the computation and experiment in order to account for the uncertainty in

the location of the microwave pulse in the experiment. This resulted in a $+10\mu$s shift in the computed pressure. The upstream undisturbed centerline pressure levels were also aligned to simplify comparison of the pressure variation between computation and experiment, implying a correction of 4 Torr and 7 Torr for Grid Nos. 1 and 2, respectively. The agreement between the computed and experimental surface pressure is good. The finer grid solution agrees more closely with the experiment. The maximum experimental pressure decrease is 30 Torr, and the maximum predicted pressure decrease (Grid No. 2) is 23.4 Torr. The effect of the filtering on the computed centerline pressure for Grid No. 2 is shown in Fig. 18. The filtering significantly reduces the magnitude of the computed pressure drop associated with the interaction of the microwave-generated plasma and the hemisphere cylinder.

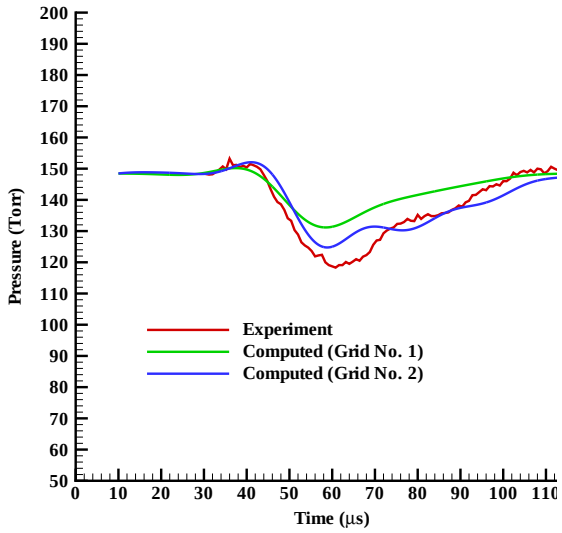

Figure 17. Centerline pressure

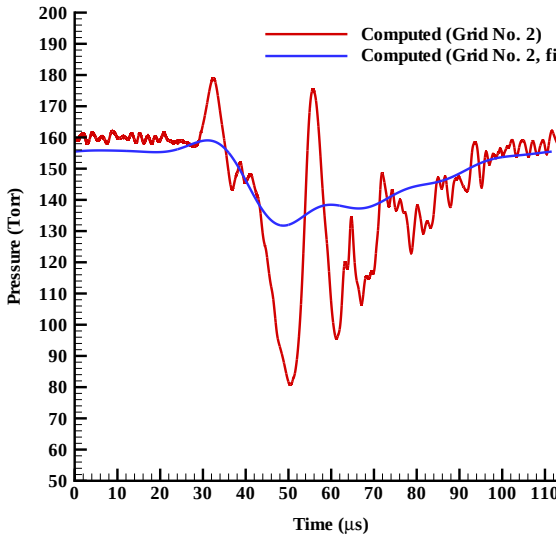

Figure 18. Centerline pressure

B. Plasma Interaction with Hemisphere-Cone Cylinder

The gas dynamic code is applied to the simulation of the interaction of a microwave-generated plasma with the flow past a hemisphere-cone-cylinder. The flow configuration is shown in Fig. 19 and corresponds to experiments.[18] The microwave pulse is focused at a distance x_o upstream of the center of curvature of the hemisphere. The freestream conditions are shown in Table 5 and the microwave parameters in Table 6. The freestream species concentrations for N_2 and O_2 correspond to standard air at the specified static pressure and temperature. A small freestream concentration of electrons N_e and molecular oxygen ions $N_{O_2^+}$ were included. The freestream concentration of all other species is set to zero. The Reynolds number based upon the cylinder diameter and freestream conditions is $Re_\infty = 2.47 \cdot 10^5$. The Prandtl number $Pr = 0.72$ and the Lewis number $Le = 1$.

Two separate computations were performed (Case Nos. 1 and 2) with different shapes of the electric field (Table 6). The cases differed in two respects. First, the streamwise length of the electric field is equal to $\frac{1}{2}\lambda$ and λ for Case Nos. 1 and 2, respectively. This is the principal difference between the two cases. Second, Case No. 1 is inviscid (since it was a preliminary computation to assess the effect of l_f), and Case No. 2 is viscous. The number of cells N_ξ

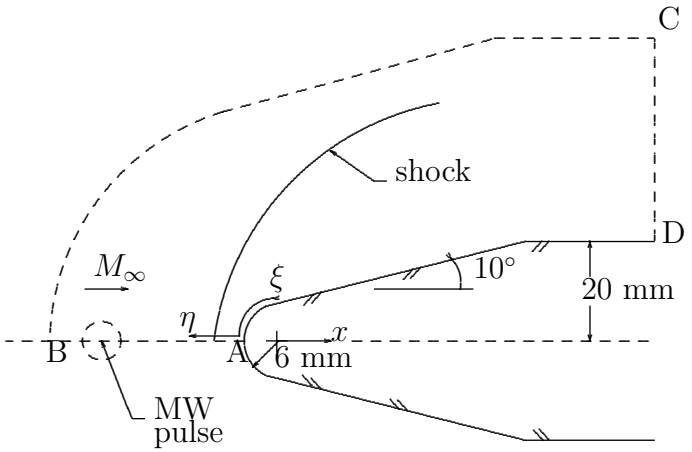

Figure 19. Computational domain

Table 5. Freestream

Quantity	*Value*
M_∞	2.1
p_∞ (Torr)	41
T_∞ (K)	153
T_w (K)	288
D (cm)	4.0
N_{N_2} (cm^{-3})	$2.044 \cdot 10^{18}$
N_{O_2} (cm^{-3})	$5.434 \cdot 10^{17}$
$N_{O_2^+}$ (cm^{-3})	$3.0 \cdot 10^4$
N_e (cm^{-3})	$3.0 \cdot 10^4$

Table 6. Microwave

Quantity	*Case 1*	*Case 2*
E_o (kV/cm)	3.35	3.35
λ (cm)	3.33	3.33
f (GHz)	9.0	9.0
τ_o (μs)	1.20	1.20
τ_1 (μs)	1.21	1.21
x_o (cm)	-2.1	-2.1
l_f (cm)	1.67	3.33
n	0	1
Model	I	V

LEGEND

I Inviscid V Viscous

Table 7. Details of Computation

Quantity	*Value*
N_ξ	350
N_η	286
N_{total}	100,100
$\Delta r_{\min}$ (cm)	$1.00 \cdot 10^{-2}$
$\Delta r_{\max}$ (cm)	$1.00 \cdot 10^{-2}$
$\Delta s_{\min}$ (cm)	$1.00 \cdot 10^{-2}$
$\Delta s_{\max}$ (cm)	$7.19 \cdot 10^{-2}$
N_p	44

and N_η in the ξ- and η-directions, respectively, are indicated, together with the total number of cells N_{total} in the computational domain in Table 7. The grid spacing Δr in the η-direction is uniform and equal to $0.0025D$. The minimum grid spacing Δs in the ξ-direction on the hemisphere cylinder is $0.0025D$ and the maximum Δs is $0.018D$. The number of processors $N_p = 44$. Axis boundary conditions are applied on the symmetry axis AB. Freestream conditions are imposed on the outer boundary BC, and zero gradient conditions at the outflow boundary CD. For Case 1, slip boundary conditions are applied on the hemisphere-cone-cylinder surface AD. For Case 2, no-slip isothermal boundary conditions are applied on the hemisphere-cone-cylinder surface AD with $T_w = 1.88T_\infty$. The semi-implicit Runge-Kutta algorithm is used in the initial stages of the computation due to the rapid increase in species concentrations and gas temperature in the region of the microwave beam during the microwave pulse. After a few microseconds of physical time, the temporal algorithm is

switched to an explicit Runge-Kutta scheme. The initial condition for the microwave pulse is the converged solution for flow past the body at the freestream conditions.

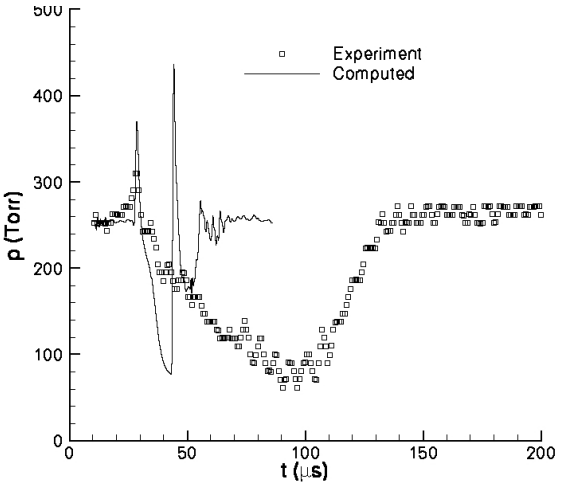

Figure 20. Case 1

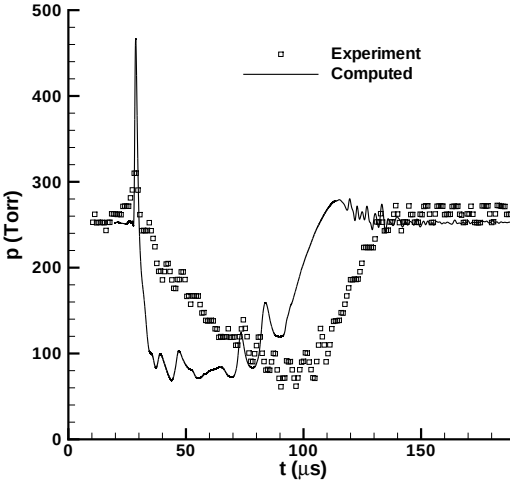

Figure 21. Case 2

The computed and experimental surface pressure *vs* time on the centerline of the body surface for the hemisphere-cone-cylinder are shown in Figs. 20 and 21 for Case Nos. 1 and 2, respectively. Due to the experimental uncertainty in the location of the microwave discharge, the timescale of the computation is shifted 10.89 μs and 19.89 μs for Case Nos. 1 and 2, respectively, to align the initial pressure rise with the experiment. The predicted minimum pressure in Case 1 shows excellent agreement with experiment. However, it is evident that the duration of the interaction is too short compared with the experiment. This implies that the streamwise length of the microwave-generated plasma is too small. The streamwise length of the plasma is sensitive to the streamwise shape ($x-$direction shape) of the electric field. For Case 1, $l_f = \frac{1}{2}\lambda$, and therefore, a greater streamwise length $l_f = \lambda$ of the electric field was assumed for Case 2. The predicted minimum pressure in Case 2 shows excellent agreement with experiment. Moreover, the duration of the pressure drop more closely agrees with experiment. Nonetheless, further research is needed to define a more accurate spatial distribution of the electric field.

Examples of the instantaneous flow structure are presented in Figs. 22 and 23. Temperature contours are displayed in Fig. 22 at $t = 28.7$ μs corresponding to the peak centerline surface pressure in Fig. 21. The time indicated in the figures includes the offset of 19.89 μs introduced in Fig. 21 to align the experimental and computed peak pressure associated with the impingement of the blast wave on the centerline surface of the hemisphere. The interaction of the heated plasma causes a lensing upstream of the blunt body shock. Contours of concentration of atomic oxygen (formed by dissociation of O_2 during the microwave discharge) are shown in Fig. 23 together with contours of static pressure at the same instant as Fig. 22. High levels of atomic oxygen are present, thus indicating the importance of modeling the flowfield chemistry associated with the microwave discharge.

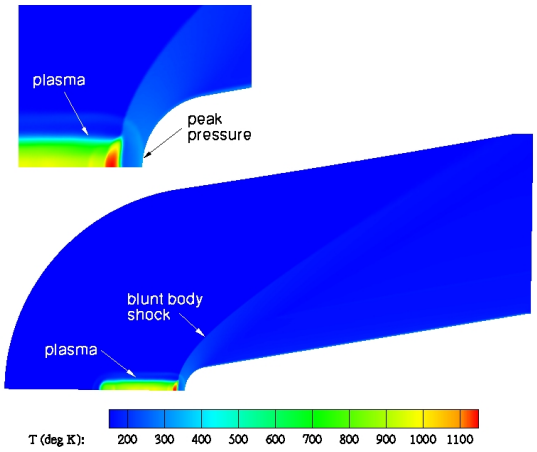

Figure 22. T **at** $t = 28.7$ μ**s**

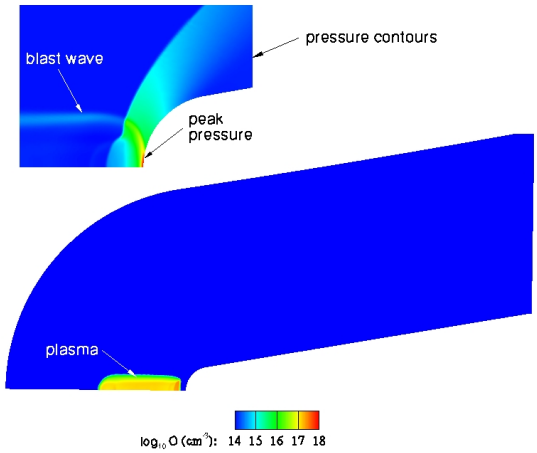

Figure 23. N_O **and** p **at** $t = 28.7$ μ**s**

IV. Publications

Zheltovodov, A., Pimonov, E. and Knight, D., "Numerical Modeling of Vortex/Shock Wave Interaction and Its Transformation by Localized Energy Deposition", *Shock Waves*, Vol. 17, 2007, pp. 273–290.

Knight, D., "Brief Survey of High Speed Flow Control Using Microwave Energy Deposition", Second European Conference for Aerospace Sciences (EUCASS), Brussels, Belgium, July 2007.

Knight, D., Kolesnichenko, Y., Brovkin, V. and Khmara, D., "High Speed Flow Control Using Microwave Energy Deposition", 16th Australasian Fluid Mechanics Conference, December 2007, Gold Coast, Australia.

Knight, D., "Survey of Aerodynamic Drag Reduction at High Speed by Energy Deposition", *Journal of Propulsion and Power*, Vol. 24, No. 6, 2008, pp. 1153–1167.

Knight, D., Kolesnichenko, Y., Brovkin, V. and Khmara, D., "High Speed Flow Control Using Microwave Energy Deposition", AIAA Paper No. 2008-1354, 2008.

Farzan, F., Knight, D., Azarova, O. and Kolesnichenko, Y., "Interaction of a Microwave Filament and Blunt Body in Supersonic Flow", AIAA Paper No. 2008-1356, 2008.

Knight, D., Brovkin, V., Khmara, D., Kolesnichenko, Y., Lashkov, V. and Mashek, I., "Interaction of a Microwave Pulse with Hemisphere Cylinder", Thermochemical Processes in Plasma Aerodynamics, St. Petersburg, Russia, May 2008.

Knight, D., Brovkin, V., Khmara, D., Kolesnichenko, Y., Lashkov, V. and Mashek, I., "Interaction of a Microwave-Generated Plasma with Flow Past a Hemisphere Cylinder at Mach 2.1", Sixth European Symposium on Aerothermodynamics of Space Vehicles, November 2008.

Knight, D., Azarova, O. and Kolesnichenko, Y., "Drag Force Control via Asymmetrical Microwave Filament Location in a Supersonic Flow", Sixth European Symposium on Aerothermodynamics of Space Vehicles, November 2008.

Aradag, S., Yan, H. and Knight, D., "The Effects of Laser Energy Deposition on Supersonic Cavity Flow", *Journal of Thermal Science and Technology*, Vol. 29, No. 2, 2009, pp. 67–73.

Knight, D., Kolesnichenko, Y., Brovkin, V., Khmara, D., Lashkov, V. and Mashek, I.,

"Interaction of Microwave-Generated Plasma with a Hemisphere Cylinder at Mach 2.1", *AIAA Journal*, Vol. 47, No. 12, 2009, pp. 2996–3010.

Knight, D., Kolesnichenko, Y., Brovkin, V., Khmara, D., Lashkov, V. and Mashek, I., "Interaction of a Microwave-Generated Plasma with a Blunt Body at Mach 2.1", AIAA Paper No. 2009-0846, 2009.

Knight, D., Azarova, O. and Kolesnichenko, Y., "On Details of Flow Control via Characteristics and Location of Microwave Filament During Its Interaction with Supersonic Blunt Body", AIAA Paper No. 2009-0847, 2009.

Norton, K. and Knight, D., "Thermal Effects of Microwave Energy Deposition in Supersonic Flow", AIAA Paper No. 2009-1224, 2009.

Knight, D., Kolesnichenko, Y., Brovkin, V., Lashkov, V. and Mashek, I., "Simulation of Microwave Energy Deposition in Air and Application to Flow Control", Eighth Workshop on Magneto-Plasma Aerodynamics, Moscow, Russia, April 2009.

Azarova, O., Kolesnichenko, Y. and Knight, D., "The Role of Instabilities with Vortices in Interaction of Heat Inhomogeneities with Supersonic Blunt Body", Eighth Workshop on Magneto-Plasma Aerodynamics, Moscow, Russia, April 2009.

Knight, D., Kolesnichenko, Y., Brovkin, V., Lashkov, V. and Mashek, I., "Interaction of a Microwave-Generated Plasma with a Blunt Body at Mach 2.1", Third European Conference for Aerospace Sciences (EUCASS), Versailles, France, July 2009.

Knight, D., Kolesnichenko, Y., Brovkin, V., Lashkov, V. and Mashek, I., "Interaction of Microwave-Generated Plasma with Hemisphere-Cone-Cylinder", AIAA Paper No. 2010-1005, 2010.

Anderson, K., and Knight, D., "Interaction of Heated Filaments with a Blunt Cylinder in Supersonic Flow", AIAA Paper No. 2010-1381, 2010.

V. Personnel

Principal Investigator: Prof. Doyle Knight
Graduate Student : Ms. Kellie Anderson (MS, Rutgers University, 2009; PhD, Rutgers University, 2012 (expected))
Graduate Student : Ms. Farnaz Farzan (MS, Rutgers University, 2008)

References

[1]Shang, J., "Recent Research in Magneto-Aerodynamics," *Progress in Aerospace Sciences*, Vol. 27, No. 1, 2001, pp. 1–20.

[2]Knight, D., Kuchinskiy, V., Kuranov, A., and Sheikin, E., "Survey of Aerodynamic Flow Control at High Speed Using Energy Addition," *AIAA Paper No. 2003-0525*, 2003.

[3]Fomin, V., Tretyakov, P., and Taran, J. P., "Flow Control Using Various Plasma and Aerodynamic Approaches," *Aerospace Science and Technology*, Vol. 8, No. 5, 2004, pp. 411–421.

[4]Knight, D., "Survey of Magneto-Gasdynamic Local Flow Control at High Speeds," *AIAA Paper No. 2004-1191*, 2004.

[5]Bletzinger, P., Ganguly, B., Van Wie, D., and Garscadden, A., "Plasmas in High Speed Aerodoynamics," *Journal Physics D: Applied Physics*, Vol. 38, No. 4, 2005, pp. R33–57.

[6]Knight, D., "Survey of Aerodynamic Drag Reduction at High Speed by Energy Deposition," *Journal of Propulsion and Power*, Vol. 24, No. 6, 2006, pp. 1153–1167.

[7]Kolesnichenko, Y., Brovkin, V., Leonov, S., Krylov, A., Lashkov, V., Mashek, I., Gorynya, A., and

Ryvkin, M., "Investigation of a AD-Body Interaction with Microwave Discharge in Supersonic Flows," *AIAA Paper No. 2001-0345*, 2001.

[8]Kolesnichenko, Y., Brovkin, V., Leonov, S., Krylov, A., Lashkov, V., Mashek, I., Gorynya, A., and Ryvkin, M., "Influence of Differently Organized Microwave Discharge on AD-Body Characteristics in Supersonic Flow," *AIAA Paper No. 2001-3060*, 2001.

[9]Kolesnichenko, Y., Brovkin, V., Azarova, O., Grudnitsky, V., Lashkov, V., and Mashek, I., "Microwave Energy Release Regimes for Drag Reduction in Supersonic Flows," *AIAA Paper No. 2002-0353*, 2002.

[10]Kolesnichenko, Y., Brovkin, V., Khmara, D., Lashkov, V., Mashek, I., and Ryvkin, M., "Microwave Discharge Parameters in Supersonic Flow," *AIAA Paper No. 2002-0356*, 2002.

[11]Wilkerson, J., Van Wie, D., and Cybyk, B., "Numerical Assessment of Heterogeneous Plasma Discharge Effects on Supersonic Forebody Drag," *AIAA Paper No. 2003-0523*, 2003.

[12]Kolesnichenko, Y., Brovkin, V., Azarova, O., Grudnitsky, V., Lashkov, V., and Mashek, I., "Microwave Energy Deposition for Aerodynamic Application," *AIAA Paper No. 2003-0361*, 2003.

[13]Anderson, K., *Interaction of Heated Filaments with a Blunt Body in Supersonic Flow*, Master's thesis, Rutgers University, Department of Mechanical and Aerospace Engineering, 2010.

[14]Van Leer, B., "Flux-Vector Splitting for the Euler Equations," *Lecture Notes in Physics*, Vol. 170, No. 82-30, 1982, pp. 507–512.

[15]Harten, A. and Chakravarthy, S., "Multi-Dimensional ENO Schemes for General Geometries," Tech. Rep. 91-76, Institue for Computer Applications in Science and Engineering, 1991.

[16]Abramowitz, M. and Stegun, I., *Handbook of Mathematical Functions*, Vol. 55, National Bureau of Standards, Washington, DC, 1971.

[17]Colella, P. and Woodward, P., "The Numerical Simulation of Two-Dimensional Fluid Flow with Strong Shocks," *Journal of Computational Physics*, Vol. 54, No. 1, 1984, pp. 115–173.

[18]Kolesnichenko, Y., Azarova, O., Brovkin, V., Khmara, D., Lashkov, V., Mashek, I., and Rivkin, M., "Basics in Beamed MW Energy Deposition for Flow/Flight Control," *AIAA Paper No. 2004-0669*, 2004.

[19]Farzan, F., Knight, D., Azarova, O., and Kolesnichenko, Y., "Interaction of Microwave Filament and Blunt Body in Supersonic Flows," *AIAA Paper No. 2008-1356*, 2008.

[20]Knight, D., Lashkov, V., and Mashek, I., "Interaction of Microwave-Generated Plasma with a Hemisphere Cylinder at Mach 2.1," *AIAA Journal*, Vol. 47, No. 14, 2009, pp. 2996–3010.

[21]Knight, D., Kolesnichenko, Y., Brovkin, V., D, K., Lashkov, V., and Mashek, I., "Interaction of Microwave-Generated Plasma with a Blunt Body at Mach 2.1," *AIAA Paper No. 2009-0846*, 2009.